RSC Advances

PAPER

View Article Online
View Journal | View Issue

Cite this: *RSC Adv.*, 2023, **13**, 734

Catalytic production of 1,2-propanediol from sucrose over a functionalized Pt/deAl-beta zeolite catalyst†

Shizhuo Wang,[a] Jikang Jiang,[a] Minyan Gu,[a] Feng Gao*[b] and Zheng Shen*[a]

To eliminate the dependence on fossil fuels and expand the applications of biomass conversion, an efficient Pt/deAl-beta@$Mg(OH)_2$ catalyst was designed, with dealuminated beta zeolite loaded with Pt as the core and $Mg(OH)_2$ as the shell. The catalyst was used to produce 1,2-propanediol (1,2-PDO) from sucrose. The preparation and reaction conditions of the catalyst were optimized. The optimal yield of 1,2-PDO was 33.5% when the conditions were 20 h of dealumination, 3.0 wt% Pt loading, 5.0 wt% $Mg(OH)_2$, 200 mg of catalyst, 10 mL (11.25 mg mL^{-1}) of sucrose solution, an initial H_2 pressure of 6 MPa, 200 °C, and 3 h. The core–shell structure of the modified beta zeolite shows good stability, yielding more than 30.0% after three cycles of reuse. Firstly, the molecular zeolite can host more acid sites after dealumination by concentrated nitric acid and this can prolong the catalyst's service life. Secondly, the loading of Pt increases the distribution of acid sites and improves the shape selectivity of the catalyst. The introduction of alkali produces many alkaline sites, inhibits the occurrence of side reactions, and increases the product yield. The above modification methods increase the production of 1,2-PDO by promoting isomerization between glucose and fructose from sucrose hydrolysis and the reverse aldol condensation (RAC) reaction. This paper provides a theoretical basis and reference route for applying biomass conversion technology in practical production, which is of great significance for developing biomass resources into high-value-added chemical products.

Received 8th November 2022
Accepted 7th December 2022

DOI: 10.1039/d2ra07097a

rsc.li/rsc-advances

1. Introduction

Biomass, as a clean and renewable resource, has been widely investigated to solve the problems of energy shortages and fossil fuel pollution. With its widely distributed nature, sucrose is one of the ideal raw materials for biomass resources.[1,2] At present, scholars have made some achievements in the research of sucrose utilization and transformation methods. Saxena prepared diatomite catalysts loaded with Ni, Mo, and Cu to obtain 28% glycerol, 22% ethylene glycol (EG), and 13% 1,2-PDO at high temperature and pressure by using sucrose as a substrate.[3] Length used copper aluminum oxide as a catalyst for the catalytic hydrogenolysis of a sucrose methanol suspension.[4] About 60% of the distillable polyols can be gathered, of which approximately 60% are 1,2-PDO. Recently, researchers have made some progress in studying the sucrose hydrogenolysis to 1,2-PDO conversion path. When exploring the conversion path of sucrose on a bifunctional Ru-POM (polyoxometalate)/AC catalyst, Garcia-Bosch found that the catalyst needs to have both a metal and an acidic function. Fructose is an essential intermediate product in the synthesis process.[5] As an important platform compound, 1,2-PDO is also a research hotspot in chemical synthesis. Previous studies on catalytic sucrose hydrogenolysis focused on the production of glycerol, EG, and 1,2-PDO and their separation, leading to a low yield of 1,2-PDO. Therefore, efficiently producing 1,2-PDO from sucrose has become of extremely high research value.

Because of their acid catalytic and structure selection ability, zeolite-modified catalysts are widely used in producing platform compounds.[6,7] Furthermore, dealumination and metal modification are commonly applied among the modification methods of beta zeolites. The acid treatment modification, as a reasonable dealumination modification, can regulate the distribution of Brønsted acid sites and Lewis acid sites in zeolites and remove non-framework aluminum from the pores of the beta zeolite.[8] Metal modification can change the acidity site distribution and pore volume of the catalysts, among which Pt loading has been a standard modification method for beta zeolite in recent years.[9–11] Under acidic conditions, glucose and fructose from sucrose hydrolysis are dehydrated to 5-hydroxymethylfurfural (HMF), and then HMF is hydrolyzed to produce

[a]*National Facility Agriculture Engineering Technology Research Center, Institute of New Rural Development, Tongji University, Shanghai 201804, China. E-mail: shenzheng@tongji.edu.cn; Tel: +86-21-65985811*

[b]*State Key Laboratory of Pollution Control and Resource Reuse, College of Environmental Science and Engineering, Tongji University, Shanghai 200092, China. E-mail: gaofeng_1111@126.com; Tel: +86-21-65985811*

† Electronic supplementary information (ESI) available. See DOI: https://doi.org/10.1039/d2ra07097a

formic acid and levopropionic acid. These side reactions reduce the yield of 1,2-PDO. Besides, acidic conditions convert fructose into lactic acid.[7] Therefore, basicity is introduced into the reaction system to inhibit the side reactions and to change the reaction path.[12] Recently, researchers have reported that the effect of using NaOH and MgO alone is limited, *e.g.*, MgO alone produced fructose with a selectivity of only 38–44% and a yield of 25%.[13] Alkali metal ion exchange treated zeolites, and metal heteroatom molecular sieves (Sn-beta molecular sieve, Ti/SiO_2, *etc.*) can efficiently play the role of alkali metals and molecular sieves, with fructose selectivities of 60–86%.[14,15] Zhu introduced WO_x into the Pd/Al_2O_3 catalyst, which enhanced the process of glucose isomerization to fructose.[16] The yield of 1,2-PDO increased to 56.1%, and the ratio of 1,2-PDO to ethylene glycol (EG) reached 10.6. They also introduced WO_x into the Cu/Al_2O_3 catalyst. Under the combined action of the catalyst, the yield of 1,2-PDO was 52.6%.[17] Many reports have focused on the study of biomass based one-step production of high value-added platform compounds. Polysaccharides are hydrolyzed into monosaccharides (*e.g.*, glucose and fructose), then converted into hexitol after isomerization and retro-aldol condensation (RAC) reaction, and finally, further dehydrated to form target compounds.[18,19] There are many studies on the preparation of lactic acid in this catalytic reaction system. Besides, lactic acid can be hydrogenated to 1,2-PDO in a hydrogen atmosphere.[9]

To improve on the traditional production methods of 1,2-PDO, we constructed a catalytic system to convert biomass into 1,2-PDO by a one-step hydrogenolysis efficiently. In this paper, a Pt/deAl-beta@$Mg(OH)_2$ core–shell catalyst was designed and prepared by dealumination, metal modification, and alkali treatment. Efficient hydrogenolysis from sucrose to 1,2-PDO is achieved by promoting isomerization and retro-aldol reaction (RAC). Pt/deAl@$Mg(OH)_2$ was synthesized by an *in situ* hydrothermal method using sucrose as the substrate and $Mg(OH)_2$ as a base. The synthesis and catalytic reaction conditions were optimized to improve the yield of 1,2-PDO catalyzed by sucrose. Then, the catalytic activities and parameters of the reaction were explored. Finally, the stability of the core–shell structure in the process of catalyst reuse was investigated. Promoting the industrialization of biomass to prepare high-value-added chemicals provides a technical route reference for research on reducing cost and increasing production.

2. Materials and methods

2.1 Materials

Sucrose ($C_{12}H_{22}O_{11}$, 99%), 1,2-PDO ($C_3H_8O_2$, 99.5%), *n*-propyl alcohol (NPA, C_3H_8O, 99.5%), ethylene glycol (EG, $C_2H_6O_2$, 99.5%), chloro-platinic acid ($H_2PtCl_6{\cdot}6H_2O$, Pt ≥ 37.5%), and a Pt standard volumetric solution were supplied by Beijing Innochem Science & Technology Co., Ltd. Nitric acid (HNO_3, GR, 65–68%), glucose ($C_6H_{12}O_6$, 99.5%), fructose ($C_6H_{12}O_6$, 99%), 1,2-hexanediol (1,2-HDO, $C_6H_{14}O_2$, 98%), magnesium oxide (MgO, 98.5%), and beta zeolite (commercial grade) were purchased from China National Pharmaceutical Group Co., Ltd.

2.2 Catalyst preparation

Beta zeolite and nitric acid were added to a three-necked round-bottom flask at a ratio of 1 g : 20 mL and mixed evenly. After the round-bottomed flask was placed in an oil bath at 80 °C, the aluminum was removed by condensation reflux (200 rpm) for 20 h. The resulting mixture (high-speed centrifuge, 3000 rpm, 20 min) was centrifuged and filtered, and the beta zeolite was rinsed with deionized water until the supernatant was neutral. The solid component (150 °C, 6 h) was dried in the oven, and the obtained powder was recorded as deAl-beta.[2]

1 g of dried deAl-beta powder was added into a 1–10 wt% Pt chloroplatinic acid solution. The mixture was stirred uniformly and then ultrasonically treated for 15 min. The sample was left to stand at room temperature and dry at 105 °C for 6 h. It was then calcinated at 450 °C for 4 h (tube furnace, air atmosphere, heating rate of 2 °C min^{-1}). After hydrothermal treatment (5 M Pa hydrogen pressure, 200 °C, 4 h), the PtO_2 supported on the catalyst was reduced to Pt. The preparation of a metal-modified dealuminated beta (deAl-beta) zeolite was completed, and denoted as Pt/deAl-beta.

50–300 mg of catalyst, 0–80 wt% MgO, and 10 mL of deionized water were added to the reactor for hydrothermal reaction (200 °C, 600 rpm, 4 h). After the reaction, the mixture was cooled to room temperature, centrifuged and filtered, and the solid was then dried in an oven to a constant weight (150 °C). In this way, the preparation of the Pt/deAl-beta@$Mg(OH)_2$ catalyst was completed.[3]

2.3 Catalytic reaction

The catalytic reaction of sucrose was carried out in a 50 mL batch reactor (Fig. S1†). It mainly comprises a control system, heating system, and reaction kettle. The reaction kettle is made of stainless steel and is equipped with a pressure gauge, temperature sensor, an inlet valve, and an outlet valve. 112.5 mg of sucrose was added to the reaction system. After three cycles of purging with 4 MPa H_2 (clean air), 6 MPa H_2 was added again and the reactor was sealed. The reaction was carried out at 180–240 °C for 1–4 h and then cooled to room temperature. The liquid-phase products and solid-phase catalysts were collected, respectively. The solid catalyst in the reactor was taken out, rinsed with excess deionized water, and dried in an oven to a constant weight (180 °C, 3 h) for reuse.

2.4 Identification of catalytic products

2.4.1 Determination by gas chromatography (GC). 1,2-PDO, EG, NPA, and other alcohol products were analyzed by gas chromatography (Agilent 7820A). The injection volume was 0.4 μL, the injection temperature was 240 °C, the detector temperature was 250 °C, the carrier gas flow rate was 20 mL min^{-1}, and the column was DB-WAXetr. The column temperature was first increased from 60 °C to 85 °C at 5 °C min^{-1}, then increased to 210 °C at 15 °C min^{-1}, then increased to 230 °C at 8 °C min^{-1}, and finally kept at a constant temperature for 3 min. The detector was FID.[4]

2.4.2 Liquid chromatography (LC). Glucose, fructose, sucrose, sorbitol, mannitol, and polyols were analyzed by a Shodex SUGAR SH1011 chromatographic column in an Agilent 1200 high-performance liquid chromatography (HPLC) instrument. Differential detectors and ultraviolet detectors were used in the test process. The injection volume was 10 μL. The mobile phase was 0.005 M sulfuric acid solution, the flow rate was set to 0.5 mL min^{-1}, and the column temperature was 55 °C.

2.5 Catalyst characterization

2.5.1 Scanning electron microscopy/transmission electron microscopy (SEM/TEM). SEM was used to observe the catalysts with a Hitachi S4800, and the TEM image of the catalysts was recorded on a JEOLJEM-1230 instrument to observe the morphology of the catalyst.

2.5.2 X-ray diffraction (XRD) analysis. XRD was used to characterize the crystal structure of the catalyst. A Bruker D8 X-ray diffractometer (40 kV, 40 mA, CuK radiation of 1.54 Å) was used to study the catalysts at room temperature. The scanning speed of the instrument was 2° min^{-1}, the scanning step was 0.02°, and the 2θ angle range was 5–90°. The characterization data were analyzed by Jade 6 software.

2.5.3 Determination of nitrogen adsorption–desorption curve. A Micromeritics ASAP2020M analyzed the specific surface area and pore size distribution of the catalysts. Before starting measurement, each sample was purged in a vacuum at 300 °C for 3 h. The specific surface area of the catalysts was calculated by the Brunauer–Emmett–Teller (BET) method, and the Barrett–Joyner–Halenda (BJH) model was used to calculate the pore volume. The physicochemical parameters of the catalysts are defined as follows: the mesoporous specific surface area (S_{meso}) was calculated using the desorption branch and BJH method, the total pore volume (V_{total}) was measured at $P/P_0 = 0.95$, and the pore size (D_{pore}) was calculated using the desorption branch and BJH method.

2.5.4 Carbon dioxide temperature programmed desorption (CO_2-TPD). The basicity of the catalysts was determined by CO_2-TPD. Using a Micromeritics AutochemII 2920, the catalyst was dried in argon to remove surface gas and water, and saturated CO_2 was adsorbed at room temperature. Then, the temperature was programmed at 10 °C min^{-1} under an argon flow rate of 30 cm^3 min^{-1}, and the amount of CO_2 desorbed from 45 °C to 800 °C was recorded by the TCD detector.

2.5.5 Temperature programmed desorption analysis of ammonia (NH_3-TPD). The acidity of the catalysts was determined by NH_3-TPD. Using a Micromeritics AutochemII 2920, the catalyst was dried in argon to remove surface gas and water, and saturated NH_3 was adsorbed at room temperature. Then, the temperature was programmed at 10 °C min^{-1} under the condition of an argon flux of 30 cm^3 min^{-1}, and the desorbed amount of NH_3 from 45 °C to 800 °C was recorded by the TCD detector.

2.5.6 Infra-red spectroscopy of pyridine adsorption (Py-IR). The acid species and the number of acid sites of the catalysts were determined by Fourier transform infrared spectroscopy (PerkinElmer Frontier, FT-IR). The spectrometer has a recording range of 1400–1700 cm^{-1} and a resolution of 2 cm^{-1}. The sample was dried in a vacuum at 450 °C for 2 h before testing. After cooling to room temperature, pyridine vapor was moved into the sample chamber to allow the sample to fully adsorb pyridine for 0.5 h. Then, the sample chamber was heated to 150 °C, 250 °C, 350 °C, and 450 °C, respectively, and stabilized for 1 h. The amount of pyridine was analyzed by an infrared quantitative test.

2.6 Calculation

Sucrose conversion (%) was defined as:

$$\text{conversion}(\%) = \frac{\text{moles of sucrose after reaction}}{\text{moles of sucrose before reaction}} \times 100\%$$

The yield of products (%) was defined as:

$$\text{yield}(\%) = \frac{\text{the number of carbon atoms in the product molecule} \times \text{moles of product}}{6 \times \text{moles of sucrose before reaction}} \times 100\%$$

3. Results and discussion

3.1 Synthesis and characterization of the catalyst

3.1.1 Structural properties. As shown by the TEM analysis of the catalysts in Fig. 1, the Pt nanoparticles are uniformly distributed on the beta zeolites with a size of about 5 nm. The lattice spacing of Pt is 0.227 nm, which is consistent with the Pt (111) crystal plane data. Compared with Pt/deAl-beta, Pt particles of the prepared catalysts by *in situ* hydrothermal synthesis have a higher dispersion and smaller particle size. Due to the many free hydroxyl groups available under hydrothermal conditions, MgO precursors can be converted mainly to $Mg(OH)_2$.[16] After the hydrothermal reaction, Pt/deAl-beta was wrapped in a shell with a thickness of 10–40 nm. A complete catalyst particle shape can be observed clearly in the SEM analysis, with $Mg(OH)_2$ embedded in flakes around the Pt/deAl-beta particles (Fig. 1(c)). The synthesis of the Pt/deAl-beta@$Mg(OH)_2$ core–shell structure includes three main steps. First, the precursor MgO was hydrated to $Mg(OH)_2$ under hydrothermal conditions.[17] Then, $Mg(OH)_2$ is dissociated into Mg^{2+} and OH^-, and rearranged into flakes.[18] Pt particles are exposed to the surface of the core–shell structure when $Mg(OH)_2$ ionizes excess OH^-, which causes more significant

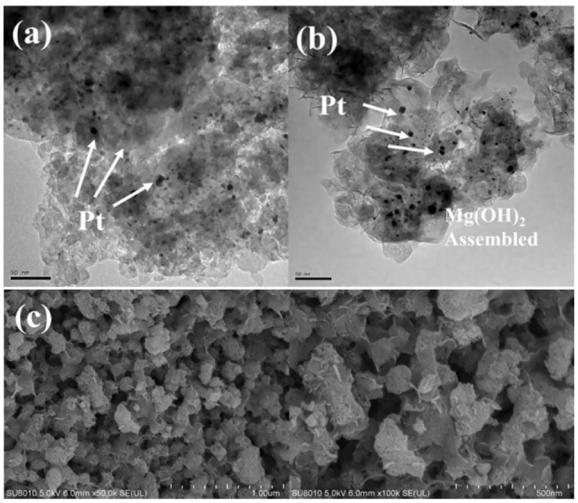

Fig. 1 TEM images of (a) Pt/deAl-beta and (b) Pt/deAl-beta@$Mg(OH)_2$, and SEM images of (c) Pt/deAl-beta@$Mg(OH)_2$.

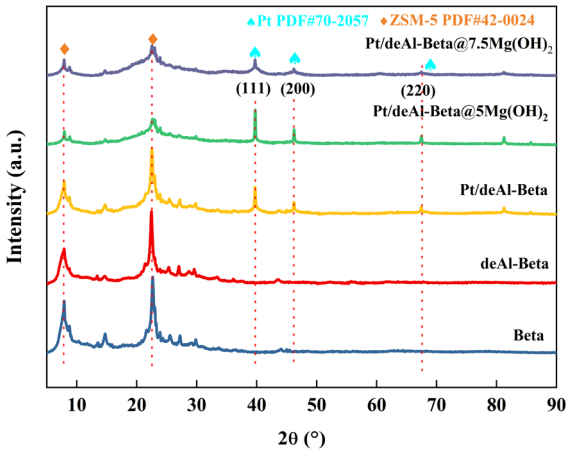

Fig. 2 The nitrogen adsorption–desorption isotherms of different catalysts.

agglomeration and loss. Finally, the alkali is corroded at high temperature and embedded on the catalyst surface. After the hydrothermal reaction, $Mg(OH)_2$ was successfully assembled on the dealuminated and Pt-loaded beta zeolite to form the Pt/deAl-beta@$Mg(OH)_2$ core–shell structure. Wang obtained the core–shell structure by adding additional alkaline substances to the system to promote the shell growth of the catalyst.[19] The basicity of $Mg(OH)_2$ without additional alkali was used to promote the formation of the core–shell structure.

3.1.2 Textural properties. The pore structure of the catalysts was explored using the nitrogen adsorption–desorption curve. The Pt/deAl-beta and Pt/deAl-beta@$Mg(OH)_2$ catalysts have two hysteresis loops at relative pressures of $P/P_0 < 0.01$ and $0.4 < P/P_0 < 0.9$, corresponding to type I and IV isotherms, respectively. This suggests that both micropores and mesopores exist in the catalyst (Fig. S2†). After alkali modification, the hysteresis loop of Pt/deAl-beta becomes more extensive and is positively correlated with $Mg(OH)_2$ loading, which confirms that the pore volume of mesopores increases to a certain extent. Mesopores are created by $Mg(OH)_2$, which helps disperse the Pt particles (Table 1).

The crystal structures of beta, deAl-beta, Pt/deAl-beta, and Pt/deAl-beta@$Mg(OH)_2$ were analyzed by using XRD (Fig. 2). The diffraction peaks of Pt completely matched the Pt (111), (200), and (220) crystal planes in the JCPDS no. 70-2057 card, indicating that the modified beta zeolites do not undergo severe skeleton collapse. Pt was successfully loaded onto the catalyst. After loading $Mg(OH)_2$, the half-peak widths of Pt (111) and (200) increased, confirming that the $Mg(OH)_2$ shell increases the dispersion of Pt nanoparticles under hydrothermal conditions and effectively inhibits the agglomeration of Pt nanoparticles. There was no peak of $Mg(OH)_2$ in the XRD pattern, and it was inferred that $Mg(OH)_2$ covered the surface of the beta zeolite in an amorphous manner. Comparing the catalysts with different loadings of $Mg(OH)_2$, it can be found that the diffraction peak intensity decreases to a certain extent with the increase of $Mg(OH)_2$ loading. It is speculated that a high $Mg(OH)_2$ loading will form a thicker shell structure on the surface of the catalyst, which will strengthen the shielding effect on the crystal.

3.1.3 Acid–base properties. The alkalinity of the modified beta zeolites with different treatment methods was analyzed by CO_2-TPD. According to the desorption curve of MgO, Pt/deAl-beta loaded with $Mg(OH)_2$ showed two desorption peaks at 100 °C and 750 °C, representing weak alkaline sites and strong alkaline sites, respectively (Fig. 3). The peak of CO_2 desorption at lower temperatures is due to the adsorption of CO_2 as carbonates on the hydroxyl groups on the $Mg(OH)_2$ surface. At higher temperatures, the desorption of CO_2 is expected from the

Table 1 The pore properties of the prepared catalysts

Catalyst	S_{BET}[a] ($m^2\ g^{-1}$)	S_{meso}[b] ($m^2\ g^{-1}$)	V_{micro}[c] ($cm^3\ g^{-1}$)	V_{meso}[d] ($cm^3\ g^{-1}$)	D_{ave}[e] (nm)	D_{meso}[f] (nm)
Beta	428	134	0.36	0.36	3	11
deAl-beta	412	138	0.37	0.38	4	11
Pt/deAl-beta	302	116	0.33	0.41	4	14
Pt/deAl-beta@5.0$Mg(OH)_2$*	139	102	0.18	0.25	5	10
Pt/deAl-beta@7.5$Mg(OH)_2$*	230	177	0.26	0.37	5	8

[a] BET surface area. [b] BJH adsorption cumulative surface area of pores. [c] Single point adsorption total pore volume of pores at $P/P_0 = 0.95$. [d] BJH adsorption cumulative volume of pores. [e] Adsorption average pore diameter by BET. [f] BJH adsorption average pore diameter. * The number represents the mass fraction of $Mg(OH)_2$ loading.

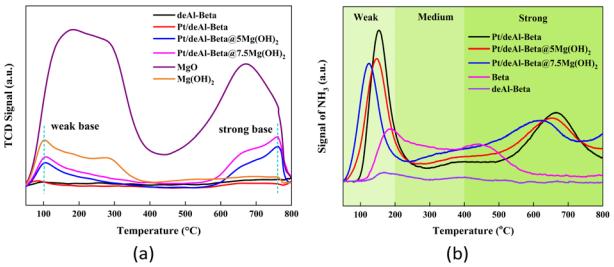

Fig. 3 (a) CO_2-TPD and (b) NH_3-TPD results for different catalysts.

single and double-coordination carbonates on the surface of MgO.[18] After the alkali modification of the Pt/deAl-beta catalyst, the number of alkaline sites was dramatically improved, mainly concentrated in weak and strong alkaline sites. With the increase of alkali loading, the strength of alkaline sites increases, which provides a theoretical basis for alkali modification.

The Pt/deAl-beta@$Mg(OH)_2$ catalyst has a unique shell–core structure, which combines the characteristics of Pt-based materials and $Mg(OH)_2$, so it has excellent acidic sites and basic sites.[20] Pyridine adsorption infrared (Py-IR) can be used to characterize the type and number of acid sites. Changes in the acid sites of the catalysts were analyzed using Py-IR, and the proportion of Lewis and strong acid sites and the total acid amount gradually increased with increasing alkaline loading (Table S1† and Fig. 3(b)). When the loading amount of $Mg(OH)_2$ was 5.0 wt%, the number of weak acid sites and total acid amount of the catalyst decreased compared to Pt/deAl-beta. Appropriate alkaline loading can adjust the distribution of acidic sites in the catalyst. When the catalyst loading of $Mg(OH)_2$ is 5.0 wt%, the lower Lewis acid amount and total acid amount are beneficial to converting sucrose to 1,2-PDO because only half of the glucose is produced after sucrose hydrolysis.[5]

3.2 Catalytic properties

3.2.1 Effect of dealumination time. The reaction efficiency of the catalysts with dealumination times of 0 h (molar ratio of SiO_2/Al_2O_3 is 25 : 1), 10 h (molar ratio of SiO_2/Al_2O_3 is more than 1700 : 1), and 20 h were tested, respectively. Fig. 4 shows the yield results of 1,2-PDO, EG and NPA catalyzed by Pt/beta@$Mg(OH)_2$ (control group), Pt/deAl-beta$_{(10)}$@$Mg(OH)_2$, and Pt/deAl-beta$_{(20)}$@$Mg(OH)_2$. The yields of 1,2-PDO and EG were 29.3%, 29.8%, and 29.1%, and 5.1%, 6.2%, and 6.0%, respectively. Under the catalytic effect of Pt/deAl-beta(10)@$Mg(OH)_2$, the yield of NPA (main by-product) was 3.3%, which was much higher than 0.6% and 0.7% of the other two groups, suggesting that 1,2-PDO was more easily dehydrogenated to NPA under the catalysis of Pt/deAl-beta$_{(10)}$@$Mg(OH)_2$. In light of the yields of the target product, 1,2-PDO, and the by-product NPA, we used Pt/deAl-beta$_{(20)}$@$Mg(OH)_2$ for the experiment, and abbreviated it as Pt/deAl-beta@$Mg(OH)_2$.

3.2.2 Effect of Pt loading. The catalytic performance of $Mg(OH)_2$-loaded (5.0 wt%) and $Mg(OH)_2$-unloaded Pt catalysts

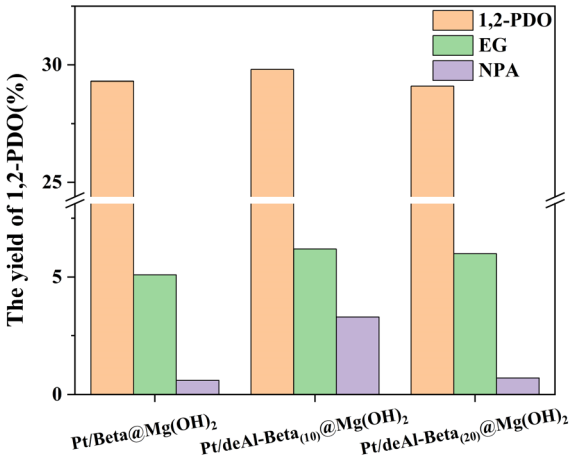

Fig. 4 The effect of beta zeolite dealumination time on sucrose hydrogenolysis into 1,2-PDO, EG, and NPA. Reaction conditions: catalyst (200 mg), Pt loading (3.0 wt%), $Mg(OH)_2$ loading (5.0 wt%), sucrose (11.25 mg mL^{-1}, 10 mL), and H_2 (initial 6 MPa) at 200 °C for 3 h. The subscript number represents the dealumination time.

with different Pt loadings was investigated using sucrose as the substrate (Fig. 5).[17] When the Pt loading was 3.0 wt%, the yield of 1,2-PDO increased by 29.5%. Upon comparing the yields of 1,2-PDO under different Pt loadings, it can be confirmed that when $Mg(OH)_2$ is not loaded, the Pt loading has little effect on the yield of 1,2-PDO, which is always maintained at about 4.0%. After loading $Mg(OH)_2$, the yield of 1,2-PDO increased significantly due to the loading of Pt. When the loading of Pt was 1.0 wt%, the yield increased by 22.8%. Then, with the increase of Pt loading, the yield of 1,2-PDO gradually rose until the Pt loading was 3.0 wt%, reaching a maximum of 33.5%. When the Pt loading exceeds 3.0 wt%, the catalytic ability of the system gradually decreases. The loading of Pt provides a hydrogen spillover effect, providing Lewis acidity for sucrose hydrolysis, which leads to an improvement of sucrose conversion.[21] The

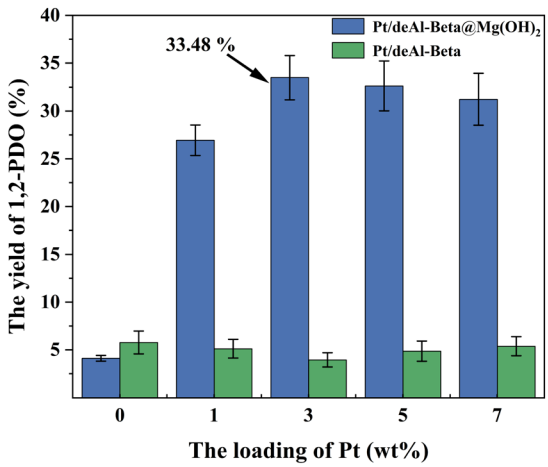

Fig. 5 The effect of Pt loading on sucrose hydrogenolysis into 1,2-PDO. Reaction conditions: catalyst (200 mg), sucrose (11.25 mg mL^{-1}, 10 mL), and H_2 (initial 6 MPa) at 200 °C for 3 h.

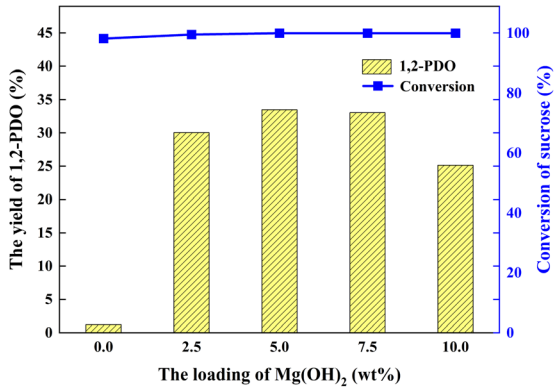

Fig. 6 The effect of $Mg(OH)_2$ loading on sucrose hydrogenolysis. Reaction conditions: catalyst (200 mg), sucrose (11.25 mg mL^{-1}, 10 mL), and H_2 (initial 6 M Pa) at 200 °C for 3 h.

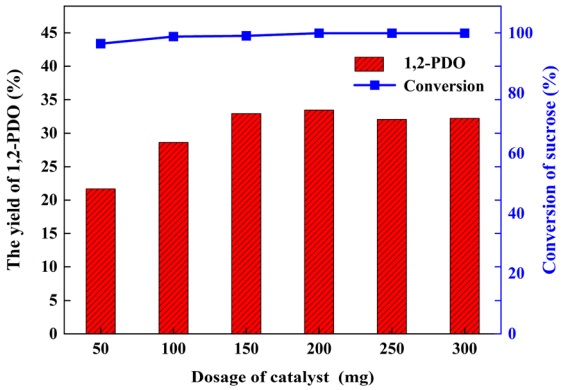

Fig. 8 The effect of catalyst dosage on sucrose hydrogenolysis into 1,2-PDO. Reaction conditions: Pt loading (3.0 wt%), sucrose (11.25 mg mL^{-1}, 10 mL), and H_2 (initial 6 MPa) at 200 °C for 3 h.

number of Lewis acid sites provided by 3.0 wt%. Pt is the most favorable for producing 1,2-PDO relative to other loadings. Low Pt loading cannot provide enough Lewis acidity, which makes the system lack the reaction power of sucrose hydrolysis and subsequent catalytic reaction. Excessive Pt loading enhances the agglomeration of Pt and blocks the pore structure of the zeolites.

3.2.3 Effect of $Mg(OH)_2$ loading. When the $Mg(OH)_2$ loading of the catalyst increased from 0 to 2.5 wt%, the yield of 1,2-PDO increased rapidly, being approximately 24 times that of $Mg(OH)_2$-unloaded, suggesting that the introduction of $Mg(OH)_2$ can indeed accelerate the formation of 1,2-PDO (Fig. 6). The yield of 1,2-PDO was improved by the $Mg(OH)_2$ loading and reached the maximum of 33.5% when the loading of $Mg(OH)_2$ was 5.0 wt%. When the loading of $Mg(OH)_2$ was 10.0 wt%, the yield of 1,2-PDO was only 25.1%, suggesting that insufficient or excessive $Mg(OH)_2$ loading was not conducive to the formation of the product. Based on the above analysis, the optimal loading of $Mg(OH)_2$ in the catalyst under these reaction conditions is 5.0 wt%.[22]

3.2.4 Optimization of reaction conditions. In the 3Pt/deAl-beta@5$Mg(OH)_2$ catalytic system, when the temperature increased from 180 °C to 200 °C, the overall yield of 1,2-PDO increased to some extent and reached the highest yield of 33.5% at the reaction time of 3 hours (Fig. 7(a)). When the temperature was further increased to 240 °C, the overall yield of 1,2-PDO was significantly reduced, being less than 15.0%. Temperature also has a significant influence on the yield of NPA. A higher reaction temperature and longer reaction time will promote the production of NPA. The yield of NPA was as high as 16.0% at 240 °C (Fig. 7(b)). Appropriately increasing the temperature can improve the reaction activity and facilitate the formation of 1,2-PDO. In contrast, a high temperature will lead to further hydrogenation of 1,2-PDO to NPA, reducing the yield. In summary, the reaction temperature of 200 °C and the reaction time of 3 h are the optimal reaction conditions for the production of 1,2-PDO in the Pt/deAl-beta@$Mg(OH)_2$ catalytic system.

During the 3 h process, when the catalyst dosage increased from 50 mg to 200 mg, the yield of 1,2-PDO rose significantly from 21.7% to 33.5%. With the continuous improvement of catalyst dosage, the yield of 1,2-PDO is generally improved. From the perspective of economic feasibility, it can be determined that the optimal dosage of Pt/deAl-beta@$Mg(OH)_2$ catalyst in this study is 200 mg (Fig. 8).

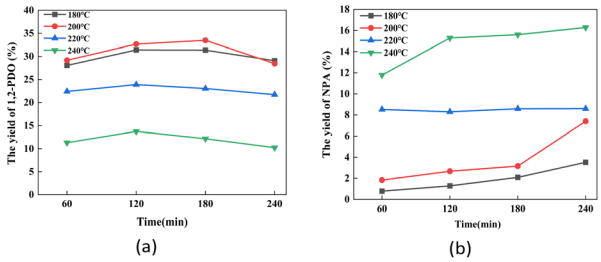

Fig. 7 The effect of reaction time on sucrose hydrogenolysis into (a) 1,2-PDO and (b) NPA. Reaction conditions: catalyst (200 mg), sucrose (11.25 mg mL^{-1}, 10 mL), and H_2 (initial 6 MPa).

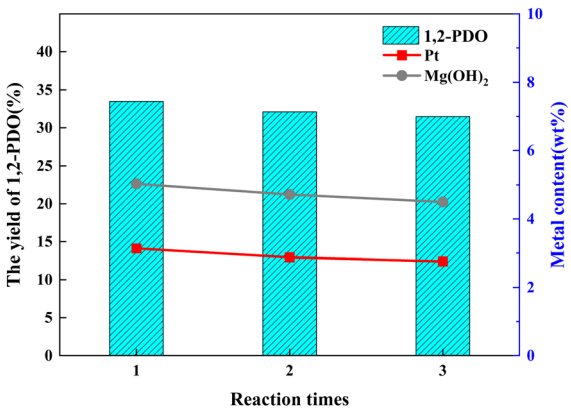

Fig. 9 Reusability and metal leaching of Pt/deAl-beta@$Mg(OH)_2$ (reaction conditions: 200 mg of Pt/deAl-beta@$Mg(OH)_2$, 10 mL of water, 112.5 mg of sucrose, 6 MPa initial H_2 pressure, 200 °C, 3 h).

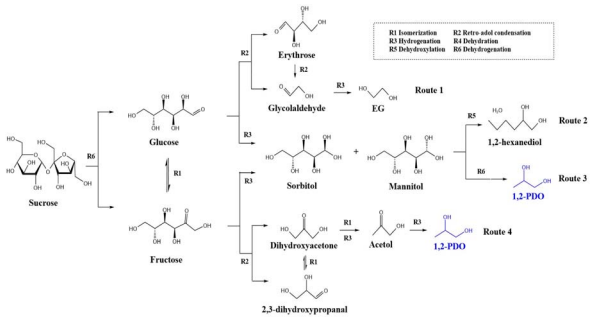

Fig. 10 The possible reaction routes of sucrose into other products.

3.2.5 Catalyst stability. During the second and third reactions of the catalyst, the yield of 1,2-PDO decreased slightly from 33.5% to 32.1% and 31.5%, respectively, suggesting that the prepared core–shell structure catalyst has stable recycling performance (Fig. 9). The yield of sucrose and the selectivity of 1,2-PDO were not significantly reduced after the catalyst was reused three times. It can be reported from the data on the right hand side that the Pt loading decreased slightly from 3.1 wt% to 2.9 wt% and 2.8 wt%, while the $Mg(OH)_2$ loading only decreased by 0.5 wt% three times with repeated use.[23]

3.3 Analysis of the catalytic reaction mechanism

Sucrose is first converted to fructose and glucose by hydrolysis. Glucose can be converted to fructose by isomerization (Fig. 10).[24] On the one hand, glucose produces erythrose and glycolaldehyde by RAC reaction. As the reaction proceeds, EG will eventually be generated (Route 1). On the other hand, fructose is converted to dihydroxyacetone (DHA) and 2,3-dihydroxypropanal (2,3-DHA) through the RAC reaction. In a hydrogen atmosphere, dihydroxyacetone finally produced 1,2-PDO by hydrogenation (Route 4). Besides, glucose and fructose can produce sorbitol and mannitol directly by hydrogenolysis. Then, hexitol is converted to 1,2-PDO by isomerization and RAC reaction (Route 3).[25,26] The improvement caused by $Mg(OH)_2$ in producing 1,2-PDO is due to three factors: the promotion of isomerization, RAC reaction, and the reconversion of hexitol.[27,28]

4. Conclusions

In this paper, based on the existing modified beta zeolite one-step catalytic process, to increase the production of 1,2-PDO from sucrose, the catalyst preparation parameters (dealumination time, Pt loading, and $Mg(OH)_2$ loading) were adjusted. At the same time, the catalyst dosage, reaction temperature, and reaction time were optimized for the catalytic process. The optimal conditions were determined: Pt loading: 3.0 wt%, $Mg(OH)_2$ loading: 5.0 wt%, catalyst: 200 mg, sucrose solution: 10 mL (11.25 mg mL^{-1}), H_2 initial pressure: 6 MPa, reaction temperature: 200 °C, and reaction time: 3 h. The optimal yield of 1,2-PDO was 33.5%. From the characterization results of CO_2-TPD and NH_3-TPD, it can be reported that after $Mg(OH)_2$ loading, the acid sites are converted to medium and strong acid sites, and weak and strong alkaline sites are produced in large quantities. The characterization results of XRD show that the shell structure of $Mg(OH)_2$ does not entirely block the reaction sites of Pt nanoparticles, which explains why the catalytic system can have both acid and alkali catalytic ability. Finally, the recycling performance of the catalyst was explored, and the structural advantages of the Pt/deAl-beta@$Mg(OH)_2$ catalyst were verified: the unique shell–core structure can effectively prevent the loss of supported metals and increase the structural stability of the catalyst.

Author contributions

Conceptualization, Zheng Shen and Feng Gao; methodology, Shizhuo Wang, Jikang Jiang, and Minyan Gu; validation, Zheng Shen and Feng Gao; data curation, Shizhuo Wang and Jikang Jiang; writing—original draft preparation, Shizhuo Wang; writing—review and editing, Shizhuo Wang , Zheng Shen and Feng Gao; formal analysis, Shizhuo Wang; supervision, Zheng Shen and Feng Gao; project administration, Zheng Shen and Feng Gao.

Conflicts of interest

There are no conflicts to declare.

Acknowledgements

This work was supported by the National Natural Science Foundation of China (No. 21978224, U21A20322), Shanghai Science & Technology Committee (No. 21dz1202400, 22dz1209300) and Key Projects of Intergovernmental International Scientific and Technological Innovation Cooperation (2022YFE0120600).

Notes and references

1 M. Morales, P. Y. Dapsens, I. Giovinazzo, J. Witte, C. Mondelli, S. Papadokonstantakis, K. Hungerbühler and J. Pérez-Ramírez, *Energy Environ. Sci.*, 2015, **8**, 558–567.
2 M. S. Holm, S. Saravanamurugan and E. Taarning, *Science*, 2010, **328**, 602–605.
3 U. Saxena, N. Dwivedi and S. R. Vidyarthi, *Ind. Eng. Chem. Res.*, 2005, **44**, 1466–1473.
4 C. Lenth and R. DuPuis, *Ind. Eng. Chem.*, 1945, **37**, 152–157.
5 N. García-Bosch, C. Especel, A. G. Ruiz and I. Rodríguez-Ramos, *Catal. Today*, 2020, **357**, 113–121.
6 M. Xia, W. Dong, M. Gu, C. Chang, Z. Shen and Y. Zhang, *RSC Adv.*, 2018, **8**, 8965–8975.
7 W. Dong, Z. Shen, B. Peng, M. Gu, X. Zhou, B. Xiang and Y. Zhang, *Sci. Rep.*, 2016, **6**, 1–8.
8 M. D. González, Y. Cesteros and P. Salagre, *Microporous Mesoporous Mater.*, 2011, **144**, 162–170.
9 S. Wang, J. Jiang, M. Gu, Y. Song, J. Zhao, Z. Shen, X. Zhou and Y. Zhang, *Nanomaterials*, 2022, **12**, 3771.
10 C. Liu, J. M. Carraher, J. L. Swedberg, C. R. Herndon, C. N. Fleitman and J.-P. Tessonnier, *ACS Catal.*, 2014, **4**, 4295–4298.

11 H. W. Lee, J.-K. Jeon, K.-E. Jeong, C.-U. Kim, S.-Y. Jeong, J. Han and Y.-K. Park, *Chem. Eng. J.*, 2013, **232**, 111–117.
12 X. Wang, Y. Song, C. Huang, F. Liang and B. Chen, *Green Chem.*, 2014, **16**, 4234–4240.
13 A. A. Marianou, C. M. Michailof, A. Pineda, E. F. Iliopoulou, K. S. Triantafyllidis and A. A. Lappas, *ChemCatChem*, 2016, **8**, 1100–1110.
14 J. M. Carraher, C. N. Fleitman and J.-P. Tessonnier, *ACS Catal.*, 2015, **5**, 3162–3173.
15 I. Delidovich and R. Palkovits, *ChemSusChem*, 2016, **9**, 547–561.
16 C. Liu, C. Zhang, S. Sun, K. Liu, S. Hao, J. Xu, Y. Zhu and Y. Li, *ACS Catal.*, 2015, **5**, 4612–4623.
17 C. Liu, C. Zhang, S. Hao, S. Sun, K. Liu, J. Xu, Y. Zhu and Y. Li, *Catal. Today*, 2016, **261**, 116–127.
18 M. Xia, W. Dong, Z. Shen, S. Xiao, W. Chen, M. Gu and Y. Zhang, *Sustainable Energy Fuels*, 2020, **4**, 5327–5338.
19 M. Xia, Z. Shen, S. Xiao, B.-y. Peng, M. Gu, W. Dong and Y. Zhang, *Appl. Catal., A*, 2019, **583**, 117126.
20 B. Y. Peng, Y. Su, Z. Chen, J. Chen, X. Zhou, M. E. Benbow, C. S. Criddle, W. M. Wu and Y. Zhang, *Environ. Sci. Technol.*, 2019, **53**, 5256–5265.
21 B. Y. Peng, Z. Chen, J. Chen, H. Yu, X. Zhou, C. S. Criddle, W. M. Wu and Y. Zhang, *Environ. Int.*, 2020, **145**, 106106.
22 B. Y. Peng, Z. Chen, J. Chen, X. Zhou, W. M. Wu and Y. Zhang, *J. Hazard. Mater.*, 2021, **416**, 125803.
23 V. Paixão, A. P. Carvalho, J. Rocha, A. Fernandes and A. Martins, *Microporous Mesoporous Mater.*, 2010, **131**, 350–357.
24 M. Gu, Z. Shen, W. Zhang, M. Xia, J. Jiang, W. Dong, X. Zhou and Y. Zhang, *ChemCatChem*, 2020, **12**, 3447–3452.
25 H. Chen, H. Yang, O. Omotoso, L. Ding, Y. Briker, Y. Zheng and Z. Ring, *Appl. Catal., A*, 2009, **358**, 103–109.
26 G. Liang, L. He, H. Cheng, W. Li, X. Li, C. Zhang, Y. Yu and F. Zhao, *J. Catal.*, 2014, **309**, 468–476.
27 M. Gu, Z. Shen, L. Yang, B. Peng, W. Dong, W. Zhang and Y. Zhang, *Ind. Eng. Chem. Res.*, 2017, **56**, 13572–13581.
28 M. Gu, L. Liu, Y. Nakagawa, C. Li, M. Tamura, Z. Shen, X. Zhou, Y. Zhang and K. Tomishige, *ChemSusChem*, 2021, **14**, 642–654.